Label-Free Photonic Crystal Biosensor Integrated Microfluidic Chip for Determination of Kinetic Reaction Rate Constants

Charles J. Choi, Ian D. Block, Brian Bole, David Dralle, and Brian T. Cunningham, *Senior Member, IEEE*

***Abstract*—We demonstrate a photonic crystal integrated microfluidic chip that is compatible with a 384-well microplate format for measuring kinetic reaction rate constants in high-throughput biomolecular interaction screening applications. The device enables low volume kinetic analysis of protein–protein interactions with low flow latency, and control of five analyte flow channels with a single control point. The structure is fabricated with a replica molding process that produces the submicron photonic crystal structure simultaneously with the micrometer-scale fluid channel structure. The device significantly reduces the kinetic assay time required compared with a conventional biosensor microplate in which reagents reach the active detection surface by diffusion. Using the photonic crystal sensor fluid network system, we demonstrate determination of the kinetic association/dissociation rate constants between immobilized ligands and analytes in the flow stream, using the heparin/lactoferrin system as an example.**

***Index Terms*—Biomedical transducers, flexible structures, optical resonance.**

I. Introduction

THE ABILITY to perform biochemical and cellular analysis using small reagent volumes and high measurement throughput has been one of the driving forces behind the development of microfluidic lab-on-a-chip (LOC) devices and micro-total-analysis systems (μTAS) [1]–[3]. Often, such systems are produced using microfabrication methods upon glass or silicon substrates with custom-designed interfaces that allow microliter quantities of reagents to be introduced into a system of microfluidic channels. However, within the field of pharmaceutical discovery and laboratory-based diagnostic assays, a great deal of liquid handling infrastructure currently exists for interfacing with standard 96, 384, and (more recently) 1536-well microplates. For this reason, it is desirable for a label-free biosensing system to easily integrate with these standard formats to enable high throughput in a single-use disposable format. This requirement has driven the commercial adoption of photonic crystal (PC) biosensor microplates for applications in pharmaceutical high-throughput screening for measuring protein–protein interactions [4]–[7], protein-small molecule interactions [8], cell-based assays [9], [10], and cell-drug interactions [11]. While label-free optical biosensors embedded within the bottom surface of microplate wells offer a convenient high-throughput detection system, the kinetics that drive detection of biomolecules to attach to the sensor surface is based mainly upon diffusion. Many publications have demonstrated the efficacy of biosensors interfaced with microfluidic channels as a means for obtaining detection kinetics that are limited by chemical reaction rates. These can serve as a rapid and sensitive means for characterizing ligand-analyte binding affinity constants through the rate of change of detected biosensor signal [12]–[16].

Recently, we demonstrated the co-fabrication of PC biosensors with a network of microfluidic channels in which a single nanoreplica molding step from a silicon "master" template wafer that contains the micrometer-scale surface structure for microfluidic channels and the nanometer-scale surface features for the PC biosensor structure. The resulting PC sensors and fluid channels were automatically self-aligned, and were fabricated over a 3×5 inch area on flexible plastic substrates for integration with a standard 96-well microplate. We also demonstrated a simple valveless control scheme in which some wells are designated as "control" wells for driving the introduction of immobilized ligands and detected analytes through microfluidic channels for real-time monitoring of up to 11 biochemical binding interactions in parallel with a high-resolution label-free imaging detection instrument [17]. With the device, reduction in the endpoint binding assay time was achieved, but kinetic analysis could not be effectively performed with the use of a long flow channel length (64 mm), which was required to bring analytes from the "analyte" microplate wells to the central measurement point. To ensure equal flow rate for a pneumatic pressure applied equally to all "analyte" wells, serpentine flow paths were implemented for wells with closest proximity to the measurement point. Despite these efforts, the previously reported chip exhibited flow rate differences between analyte flow channels, and limitations on the maximum achievable fluid flow rate.

In this paper, we demonstrate PC biosensor integrated microfluidic channels compatible with a 384-well microplate format. The device structure reported here enables low volume kinetic analysis of protein–protein interactions through five analyte flow channels with a single control point and offers

Manuscript received May 07, 2009; accepted August 06, 2009. Current version published October 21, 2009. This work was supported in part by the National Science Foundation under Award DMI 0328162 and 0427657. Any opinions, findings, and conclusions or recommendations expressed in this material are those of the author(s) and do not necessarily reflect the views of the National Science Foundation. This work was also supported by SRU Biosystems. The associate editor coordinating the review of this paper and approving it for publication was Dr. M. Abedin.

The authors are with the University of Illinois at Urbana–Champaign, Urbana, IL 61801 USA (e-mail: cjchoi@illinois.edu; iblock2@illinois.edu; bcunning@illinois.edu).

Color versions of one or more of the figures in this paper are available online at http://ieeexplore.ieee.org.

Digital Object Identifier 10.1109/JSEN.2009.2030666

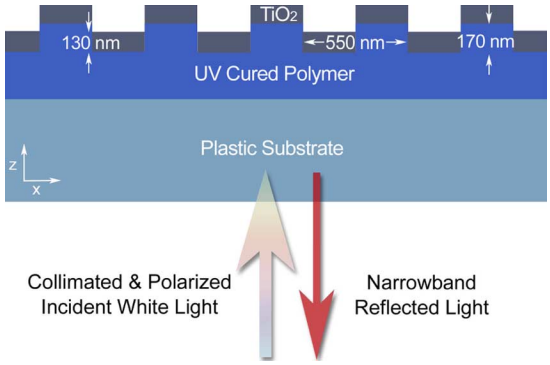

Fig. 1. Schematic cross-section diagram of the PC biosensor.

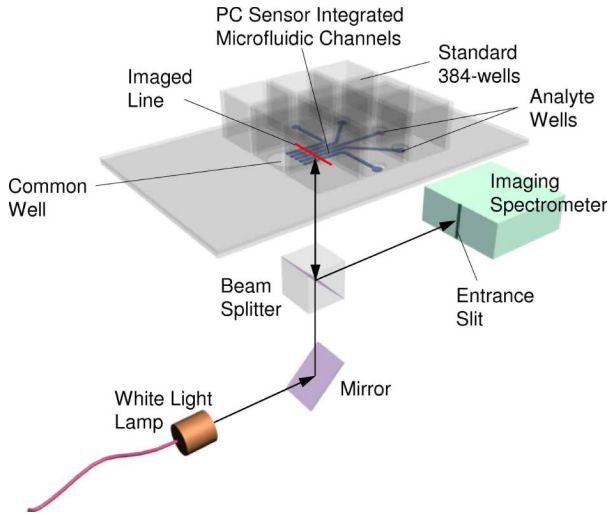

Fig. 2. Schematic of the PC biosensor integrated microfluidic assay chip with the high-resolution imaging detection instrument.

higher assay density. It is important to note that the 384-well fluid channel microplate reported here requires significantly shorter analyte travel distance from the inlet region to the PC detection region, compared to the 96-well microplate sensor format reported previously, in which kinetic analysis could not be performed effectively. This is important especially for accurate kinetic analysis of low analyte concentrations because short analyte travel distance enables very low flow latency and helps mitigate the effects of analyte molecule depletion through attachment to the channel walls before reaching the detection region. The resulting biosensor microfluidic microplate and detection instrument are capable of rapid and high-throughput characterization of biochemical binding constants in a format that is compatible with existing 384-well microplate liquid handling systems.

II. Materials and Methods

The PC shown in Fig. 1 is a nanostructure comprised of a periodically modulated low refractive index UV cured polymer linear grating coated with a high refractive index dielectric layer of titanium dioxide $(\mathrm{TiO_2})$. The device is designed to reflect only a narrow band of wavelengths with 100% efficiency when illuminated with white light at normal incidence [18]. The resonant reflection is due to evanescent diffracted orders coupling to modes of an effective high refractive index layer, which are then reradiated through diffraction in-phase with the reflected zeroth-order wave [19]. A positive shift of the reflected peak wavelength value (PWV) indicates adsorption of material on the sensor surface. Previously, PC optical biosensors have been fabricated on continuous sheets of plastic film using a process in which the periodic surface structure is replica molded directly from a silicon master wafer using a UV-cured polymer material [4]–[7], [9], [10]. The use of a continuous, roll-based, high-throughput replication process enables low-cost mass-production of large surface-area devices for single-use disposable products, capable of integration into microplates and microarray slides.

A. PC Sensor Integrated Microfluidic Chip

A schematic of the sensor-integrated microfluidic chip is shown at the top of Fig. 2. The flow channels and the PC biosensor are co-fabricated and self aligned on a single sheet of flexible plastic. A planar plastic cover is then applied over the flow channels to form the upper surface, and to provide holes for fluid access. The microfluidic network assembly is attached with adhesive to a bottomless 384-well microplate, where it forms the bottom surface. The holes on the fluid chip are arranged so that each microplate well has access to the microfluidic network through one hole. As shown in Fig. 2, the fluid channels from five "analyte" wells are gathered to a single detection region, where all five channels may be monitored at once. A "common" well serves as an access point for introduction of reagents that are identical for all of the flow channels. The common well also serves as a means for applying positive or negative pressure that will drive fluid from the common well into the flow channels, or to pull fluid from the five analyte wells at the same rate. The bends in the channels have minimal effect on the overall fluid flow rate of the channels and no flow latency between the channels was observed.

B. Device Fabrication

As in previous work, a room-temperature, low-force replica-molding process utilizing a patterned silicon master and a UV-curable polymer (Gelest, Inc.) was used to fabricate the devices [20]. The fabrication method accurately produces sub-micron features for the PC structure, while at the same time generating $> 10\ \mu\mathrm{m}$ features for the microfluidic channels in a single molding step.

First, a silicon wafer was patterned with a 550 nm period 1-D linear grating structure using deep-UV lithography and reactive ion etching to a depth of 170 nm. The fluid channels were then patterned onto the same silicon wafer using conventional contact lithography and deep reactive ion etching to a depth of $30\ \mu\mathrm{m}$. As a result of the above processing steps, a negative pattern template of microfluidic channels incorporating a submicron linear grating was fabricated. The completed silicon master was subsequently treated with dimethyl dichlorosilane (GE Healthcare) to promote clean release of the replica from the master.

Next, the master wafer pattern was replicated onto a $250\ \mu\mathrm{m}$ thick flexible polyethylene terephthalate (PET) substrate (plastic substrate in Fig. 1) by distributing a layer of liquid

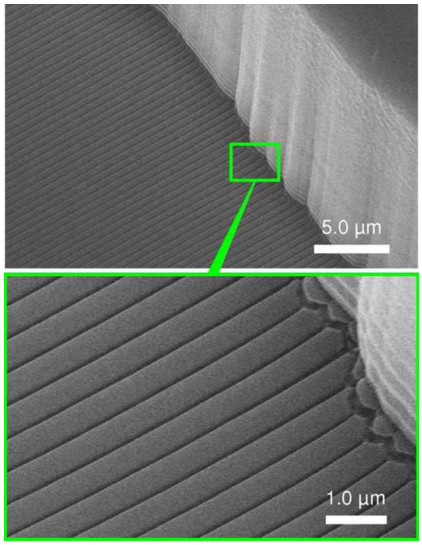

Fig. 3. SEM images of an open microfluidic channel embedded with the PC biosensor.

UV curable polymer between the silicon wafer and the PET substrate where the liquid polymer conforms to the shape of the features on the wafer. The liquid polymer was then cured to a solid state by exposure to UV light at room temperature and was subsequently released from the wafer by peeling away the PET, resulting in a polymer replica of the silicon wafer structure adhered to the PET sheet. The sensor structure was completed by depositing 130 nm of titanium dioxide $(\mathrm{TiO_2})$ on the replica surface using electron beam evaporation. For the high index layer of PC sensor structure, any dielectric material that has similar refractive index $(\mathrm{n} = 2.3)$ with low optical loss and is inert to biochemical reagents or reactions could also be used. The SEM images of the PC sensor within an open microchannel are shown in Fig. 3.

The open microfluidic channels were sealed by a separate PET sheet with die-punched 1.6 mm diameter inlet/outlet holes in a pattern corresponding to the locations of the wells of a standard 384-well microplate using a layer of double sided optically clear laminating adhesive film (3M). To complete the packaging, the fabricated polymer microfluidic network assembly was then attached to a bottomless 384-well microplate using an adhesive. The seal provided by the adhesive was very effective and no leakage of fluids occurred.

C. Detection Instrument

A schematic of the biosensor imaging instrument is shown in the bottom of Fig. 2. White light illuminates the sensor at normal incidence with polarization perpendicular to the sensor grating lines. The reflected light is directed through a beam splitter and an imaging lens to a narrow slit aperture at the input of the imaging spectrometer. Using this method, reflected light is collected from a line on the sensor surface, where the width of the imaged line is determined by the width of the entrance slit of the spectrometer. The imaging spectrometer contains a 2-D CCD chip (Acton Research) with 2048×512 pixels, in which the line image through the slit is divided into 512 pixels and a spectrum with a resolution of 2048 wavelength data points is acquired for each of the 512 pixels imaged. With a spectral measurement range of 830 to 890 nm, the detection instrument sampling interval is 0.0293 nm. Further details on the detection instrument performance specifications can be found in [21]. Upon peak-finding analysis of all 512 spectra, the PWV for each of the 512 pixels are determined, and thus a line of 512 pixels is generated for the PWV image of the sensor.

Based on the PWV imaging mechanism described above, the detection instrument is capable of operating in two different modes: kinetic mode and imaging mode. For kinetic measurements (measuring $\Delta\mathrm{PWV}$ as a function of time), a motorized stage positions the sensor so that the image line remains fixed upon a single location that intersects five flow channels (see Fig. 2), while the PWV of the PC is measured at fixed time intervals. The measurement interval can be designated by software, where the lower limit (~ 0.2 s per measurement) is determined by the integration time of the CCD chip, data analysis/routing time, and processing load on the computer. For the imaging mode (generating 2-D spatial PWV image of the sensor) however, the motorized stage translates the sensor in a direction perpendicular to the image line in small increments, constructing a spatial map of the PC PWV. By this technique, a series of lines are assembled into an image through a software program and a large area can be scanned in a serpentine tiled fashion. The PWV pixel resolution, or the line width of the imaged line for this work, was $22.3\ \mu\mathrm{m}$. The detection instrument is flexible in terms of its ability to measure reflected spectra from any PC surface, regardless of whether the PC is incorporated into stagnant microplate wells, flow channels, or continuous PC microscope slides.

D. Device Operation

Driving fluids to flow through the microchannels was accomplished by prefilling one or more microplate wells with solution, and application of pneumatic pressure. After the microplate wells were prefilled with solution, a silicone cap attached to Teflon micro tubing (Cole–Parmer) was inserted into the opening of the well and a pressure regulated lab pneumatic source (2.5 psi) was used to drive liquid through the channels.

E. Reagents

Phosphate buffered saline (PBS), Glutaraldehyde, Biotinylated heparin, and Human lactoferrin were purchased from Sigma–Aldrich. Starting Block™ blocking buffer was purchased from Pierce Biotechnology. Streptavidin was purchased from Prozyme. Amine polymer was obtained from SRU Biosystems.

III. Experiment

A. Heparin-Lactoferrin Assay

Optical biosensors employing surface binding detection are most often used to quantify the affinity of an analyte for its ligand. To provide a realistic demonstration of the assay chip for determining binding affinity between biomolecules, we investigated the sensor response to a concentration series of lactoferrin where the sensor surface is immobilized with heparin. Protein interactions with heparin mediate many biologically important

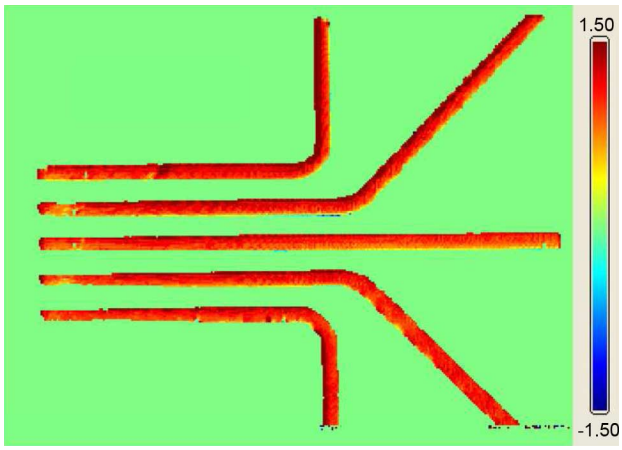

Fig. 4. Spatial PWV shift image obtained after heparin immobilization and wash. PWV shifts are represented by the color coded scale bar from -1.50 to 1.50 nm with red regions representing areas of greater positive shift.

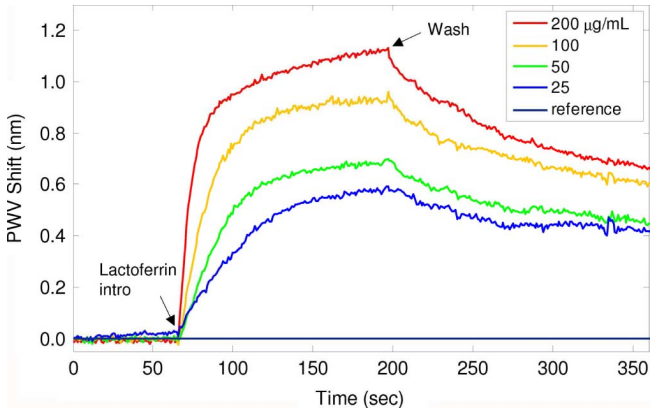

Fig. 5. Kinetic PWV response of heparin immobilized microfluidic PC sensors for lactoferrin exposure of different concentrations.

process [22]. Therefore, the characterization of the affinity and kinetics of these interactions has been of considerable interest [23]. Lactoferrin is a soluble iron-binding glycoprotein with antimicrobial and anti-inflammatory activity and heparin is a sulfated polysaccharide that comprises much of the extracellular matrix of many cell types which is used extensively as an anticoagulant drug [22], [24]. For this experiment, the heparin/lactoferrin pair was chosen because it exhibits classical association and dissociation kinetics behavior. Heparin used for the experiment was biotinylated so that it could bind to a layer of streptavidin attached to the sensor surface through a thin polymer coating and bifunctional linker, using an immobilization procedure that has been described previously [25].

Initially, the sensor-integrated microfluidic channels were washed by flowing deionized (DI) water solution from the common well into the channels. Next, the microchannels were filled with a 4% amine polymer solution in DI water and incubated at 25 °C for 24 h. After washing the channels with DI water, glutaraldehyde (25% in DI water) was flowed through and incubated at 25 °C for 2.5 h. After washing the channels with DI water, streptavidin (0.5 mg/mL in DI water) was filled and incubated at 4 °C for 24 h. The channels were then washed with DI water, followed by PBS conditioning. The capture molecule (biotinylated heparin) was then immobilized onto the sensor surfaces of all the channels by flowing the solution (0.1 mg/mL in PBS) from the common well into the channels and incubating at 4 °C for 12 h, followed by a PBS wash to remove unbound excess biotin-heparin molecules. The 2-D spatial PWV shift image after heparin immobilization/wash obtained by operating the detection instrument in the spatial imaging mode is shown in Fig. 4. The PWV shift image was acquired by subtraction of the PWV image before heparin immobilization/wash from the PWV afterwards on a pixel-by-pixel basis. PWV shifts are represented by the scale bar from -1.50 to 1.50 nm with red regions representing areas of greatest positive shift. After the heparin immobilization and wash, the unbound regions of the channels were blocked with Starting Block™ blocking buffer for 1 h. The channels were then washed with PBS solution and a concentration series of lactoferrin (200, 100, 50, 25 μg/mL in PBS) and a negative control (PBS) were added to each of the analyte wells. After the wells were preloaded with the analyte and buffer solutions, the data acquisition from the detection instrument was initiated in the kinetic mode, and the solutions were pumped from each of the analyte wells to the detection area and to the common well. At the end of the association phase, a wash step was performed by rinsing and filling the analyte wells with PBS while the solutions were continuously pumped. After the wash step, the reference channel was filled and pumped with a 2 mg/mL concentration of lactoferrin to determine the maximal binding capability of the heparin-immobilized sensor.

IV. Results

The kinetic PWV response of lactoferrin binding to the heparin-immobilized sensor is shown in Fig. 5. The width of each fluid channel was 300 μm, corresponding to 13 data pixels across (pixel resolution: 22.3 μm), but the PWV response for each channel was calculated by averaging only 7 pixels (156 μm) in the center region across the channels where the fluid flow rate was constant. We assumed that the flow rate is constant in the center region of the channel because the channel width is significantly larger than its height. The average standard deviation for the 7 pixel measurement observed was 0.0057 nm. The average PWV shift data in Fig. 5 were obtained by subtracting the average PWV of the reference channel filled with PBS buffer from the average PWV for each active channel with lactoferrin to remove effects of signal drift that are not due to heparin-lactoferrin interaction. The duration of the association/dissociation measurement was 5 min, with PWV measurements taken at 1 s intervals. A negative pressure of -2.5 psi was applied to the common well 65 s after the initiation of the PWV measurement to introduce the analyte solution over the detection area and this resulted in a fluid flow rate of 32.7 μL/min for each channel.

Based on the binding interaction between an analyte and a ligand described by the standard equilibrium reaction rate equation, change in the sensor response as a function of time is given by the ordinary dynamic surface binding equation

$$\frac{dR}{dt} = k_a [A] (R_{\max} - R) - k_d R \quad (1)$$

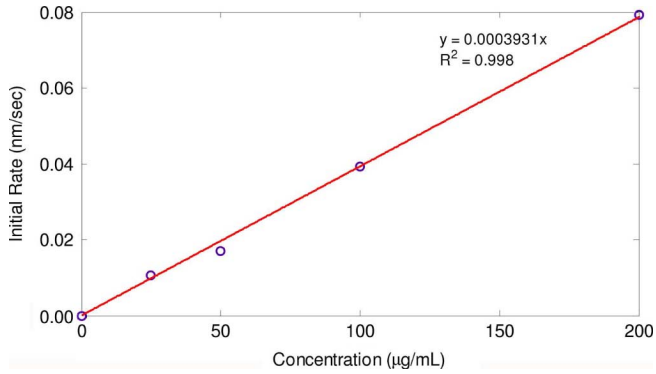

Fig. 6. Plot of initial binding rate measured between heparin and different concentrations of lactoferrin.

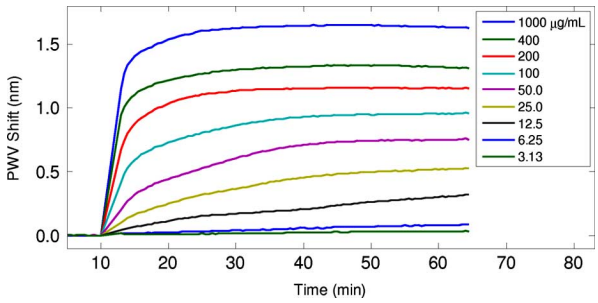

Fig. 7. Kinetic PWV response of heparin immobilized PC sensors for lactoferrin exposure of different concentrations in a standard well plate format.

where $[A]$ is the analyte concentration, $R_{\max}$ is the maximum capacity of the immobilized ligand, R is the biosensor signal which is proportional to the amount of bound molecules, k_a is the association rate constant, and k_d is the dissociation rate constant. $R_{\max} - R$ is proportional to the amount of ligand available for binding that is not already bound with analyte molecules. As shown in previous work involving biosensor output response to an analyte introduced within a flow stream, the association phase response is obtained by solving (1) at the start of the reaction $(t = 0)$ [26]

$$\left.\frac{dR}{dt}\right|_{t=0} = k_a\,[A]\,R_{\max}. \tag{2}$$

Therefore, the plot of initial sensor response rate against analyte concentration results in a linear relationship whose slope is $k_a \cdot R_{\max}$ with an intercept of zero. Using this analysis, the association rate constant between heparin and lactoferrin can be determined from the kinetic biosensor response data. Likewise, the dissociation rate constant can be determined by solving (1) during the dissociation phase where it is assumed that $[A] = 0$, resulting in the expression

$$R = (R_0 - R_\infty)\exp(-k_d t) + R_\infty \tag{3}$$

where R_0 is the sensor response at the start of the dissociation, and R_∞ is the final steady-state response. The dissociation constant, or K_D value for the heparin-lactoferrin interaction can then be determined from the relationship $K_D = k_d/k_a$.

The initial sensor response rate was determined from the kinetic binding data obtained in Fig. 5 where the rate was calculated over the linear regions of the binding curves. The initial binding data used to calculate the association rate constant ranges from 4 to 15 data points (seconds) from the initial association point. At lower concentration, the initial slope was calculated using more data points for greater precision since sensor response data at lower analyte concentrations were linear for a longer period of time. The plot of initial sensor response rate as a function of lactoferrin concentration is shown in Fig. 6. A linear fit was applied to the data using a least squares method with the y-intercept set to zero, yielding a slope $(k_a \cdot R_{\max})$ of 3.93×10^{-4} nm $(\mu\mathrm{g/mL})^{-1}\,\mathrm{sec}^{-1}$ with an R^2 value of 0.998. Using the maximum binding capability $(R_{\max})$ determined by introducing 2 mg/mL concentration of lactoferrin, the association rate constant for heparin-lactoferrin binding was calculated as $2.28 \times 10^{-4}\ (\mu\mathrm{g/mL})^{-1}\,\mathrm{sec}^{-1}$. Based on the dissociation curve fitting, the dissociation rate constant was determined to be $0.0143 \pm 6.49 \times 10^{-4}\,\mathrm{sec}^{-1}$. As a result, the K_D value for the heparin-lactoferrin interaction was determined to be $63.1 \pm 2.85\ \mu\mathrm{g/mL}$.

In order to verify the K_D value determined using the PC microfluidic assay chip, another heparin-lactoferrin assay was performed on a commercially available standard 96-well microplate PC biosensor. The biosensor microplate detection of heparin-lactoferrin binding was performed simultaneously with the microfluidic assay using the identical reagents and immobilized ligand surface preparation method. The only significant difference between the biosensor microplate assay and the flow channel assay is that the microplate assay occurs without the use of active flow, resulting in biosensor response rate that is limited by the rate of diffusion of lactoferrin to the bottom surface of the microplate well. Fig. 7 shows the kinetic PWV response of heparin immobilized PC sensors for lactoferrin exposure of different concentrations in a standard well plate format. In order to perform an endpoint concentration series assay without fluid flow, the sensor measurement had to be taken for at least 55 min until a steady-state equilibrium response is achieved. Fig. 8 depicts the endpoint PWV shift from the microplate-based sensor, 55 min after the lactoferrin introduction, as a function of lactoferrin concentration ranging from 3.13 to 1000 $\mu\mathrm{g/mL}$. The data in Fig. 8 was fit with a dose response sigmoidal curve with an R^2 value of 0.984 and the K_D value was determined to be $60.63\ \mu\mathrm{g/mL}$.

Using the PC integrated microfluidic assay chip, association/dissociation rate constants and therefore the equilibrium constant (K_D) for heparin-lactoferrin interaction was determined. To demonstrate the validity of the reaction equilibrium constant determined using the microfluidic-based PC sensor chip, an alternate method to determine the K_D value of the reaction was used on a diffusion-limited PC biosensor microplate. As shown in the experiment, the K_D value determined using the microfluidic-based PC sensor chip comes within 4.07% of the K_D range determined using the conventional microplate PC sensor.

The K_D value obtained using the PC microfluidic assay chip can also be compared to the heparin-lactoferrin interaction data previously measured using surface plasmon resonance (SPR) biosensors [23]. In that work, the analyte injection flow rate was

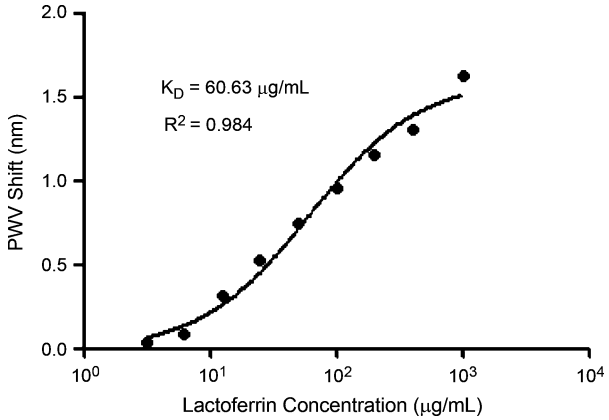

Fig. 8. Dose response curve for heparin and lactoferrin measured on a conventional wellplate-based PC sensor. Data represented as mean ± SD (error too small to be shown), $n = 3$.

$30\ \mu\mathrm{L/min}$ and the assay duration was 7 min. Based on the sigmoidal curve fitting of dose response measurement reported in the literature, the K_D value determined by SPR ranged from 10.50 to $30.94\ \mu\mathrm{g/mL}$, where K_D variation was attributed to differences in the heparin biotinylation method, (biotinylation via uronic acids, intrachain bare amines, or the reducing terminus) which, in turn, affects binding affinity for the analyte. Although a different K_D value compared to [23] was obtained from the experiment in this paper, the value is similar considering the fact that a different surface chemistry method was used.

V. Discussion

The 384-well fluid channel microplate reported here enables low volume kinetic analysis of protein–protein interactions through five analyte flow channels with a single control point and offers higher assay density format. This device requires significantly shorter analyte travel distance (5 mm) from the inlet region to the PC detection region, compared to the 96-well microplate-based microfluidic sensor format reported previously (64 mm), in which kinetic analysis could not be performed effectively. The shorter analyte travel distance becomes important for accurate kinetic analysis of low analyte concentrations because short analyte travel distance enables very low flow latency and reduces the effect of analyte molecule depletion before reaching the detection region. For the device in this paper, there was no flow latency between channels whereas with the previous 96-well plate microfluidic device, it was difficult to create low levels of f low latency (flow latency up to 7 s was observed) [17]. Ideally, the fluid flow rate among all channels should be kept identical for accurate kinetic analysis. Another consequence of long flow path length is the difference in the flow rate observed during the kinetic measurement. The analyte flow rate for the previous literature was $0.442\ \mu\mathrm{L/min}$ which is significantly lower than $32.7\ \mu\mathrm{L/min}$ for this work. A flow rate of $0.442\ \mu\mathrm{L/min}$ is too low for accurate kinetic analysis as the reaction rate becomes limited primarily by mass transport, rather than kinetic binding rate. Comparing the active surface area attached with binding sites, the previous 96-well plate-based device has 13x higher surface area available for binding compared to device presented in this paper. For lower analyte concentration assays, the level of analyte depletion due to the difference in binding site surface area becomes significant. A FEM software (COMSOL) was used to verify the difference in the kinetic binding rate between the 96 and the 384-well plate-based microfluidic channels. A difference in the kinetic binding rate was observed in the simulation even with the analyte flow rate set to be identical for both cases. With the 96-well plate microfluidic device, reduction in the endpoint binding assay time was achieved, but kinetic analysis could not be effectively achieved due to its long channel length. The biosensor microfluidic microplate presented here is not only capable of significantly reducing the assay time, but also capable characterizing biochemical kinetic binding constants accurately.

Examination of the methods used to obtain K_D for the same protein–protein interaction using the identical biosensors packaged in two different formats (microfluidic-based detection versus stagnant microplate well detection) yields interesting comparisons in terms of reagent usage and assay time. First, we compare the mass of biotinylated heparin used to generate an immobilized ligand layer in the 96-well microplate format to the mass required to prepare the microfluidic chip. For the standard 96-well biosensor microplate (SRU Biosystems)-based assay for determination of K_D, we assume five analyte (lactoferrin) concentrations are required to generate a dose-response curve, and triplicate wells are used for each concentration. Using $100\ \mu\mathrm{L}$ volumes of $100\ \mu\mathrm{g/mL}$ biotinylated heparin solution, therefore, results in the use of $150\ \mu\mathrm{g}$ of biotinylated heparin reagent. Performing heparin immobilization within three microfluidic channels, using the same concentration solution, requires only $15\ \mu\mathrm{g}$ of the ligand. One channel per concentration was used during the experiment in this work, but three channels per concentration were used to calculate reagent mass usage for comparison. This appears to be a substantial advantage for the microfluidic approach. However, biosensor microplate wells in the 384-well and 1538-well format are also available (although not used in the experiment reported here). In the 384-well microplate format, for example, only $20\ \mu\mathrm{L}$ of heparin solution would be needed to prepare each biosensor well, resulting in a heparin mass usage of $30\ \mu\mathrm{g}$, which is similar to the microfluidic mass usage. We may also compare the mass of lactoferrin analyte required for determining K_D by the two methods. For the standard 96-well microplate biosensor (SRU Biosystems), four different concentrations of lactoferrin $(25 - 200\ \mu\mathrm{g/mL})$ with triplicate wells at $100\ \mu\mathrm{L}$ volume for each well for each concentration, result in a total lactoferrin mass of $113\ \mu\mathrm{g}$. In the microfluidic experiment using the same concentrations of lactoferrin, and using a flow rate of $32.7\ \mu\mathrm{L/min}$ per channel for an assay association time of 2.2 min, and triplicate flow channels for the experiment, $81\ \mu\mathrm{g}$ of lactoferrin would be used. Therefore, the amount of analyte protein used for the microfluidic-based methods would be slightly less. For the SPR-based experiment reported in [23], the amount of lactoferrin analyte consumption would be $74\ \mu\mathrm{g}$ assuming a $30\ \mu\mathrm{L/min}$ flow rate and an assay association time of 2.2 min.

TABLE I
COMPARISON OF FLOW RATE, ANALYTE MASS REQUIRED, AND MEASURED K_D VALUE FOR DIFFERENT ASSAY PLATFORMS

	96 Well plate	Microfluidics	SPR
Flow rate (μL/min)	0	32.7	30
Analyte mass required (μg)	113	81	74
K_D value (μg/mL)	60.63	63.1 ± 2.85	10.50 to 30.94

With the standard microplate format-based biosensors, the reaction kinetics within the plate wells are dominated by the rate of diffusion of analytes to the sensor surface, unless external mixing is provided. Therefore, kinetic biosensor data do not provide reaction rate data on analyte-ligand interactions with the same utility as biosensors incorporated within microfluidic channels, where the analyte diffusion distance is significantly reduced. As a consequence, different analysis methods to determine the K_D value are used for the microplate-based format versus the microfluidic-based format. The K_D value analysis for the standard microplate format assay is based on fitting a dose-response curve (endpoint analyte concentration series assay) which requires sensor measurements to be taken until equilibrium response is reached. For the microfluidic flow-based assay however, the K_D value determination is based on fitting kinetic association and dissociation data. Therefore, both the association and dissociation rate constants (k_a and k_d) as well as the equilibrium constant (K_D) can be determined with microfluidic-based PC sensors, whereas only the K_D value can be determined with the conventional microplate-based format.

Another consequence of mass transport limitation in the standard wellplate format is the longer detection time required for the bioassay. In order to perform an endpoint concentration series assay without fluid flow, the sensor measurement has to be taken until a steady-state equilibrium response is achieved. Therefore, the K_D values of the microplate and the microfluidics-based experiments matched, but in the case of microplate-based assays, it takes more time for the equilibrium of the sensor response to be reached compared to the microfluidic assay. For the heparin-lactoferrin assay performed on a microplate sensor in this work, the assay time required for the sensor response to reach equilibrium for K_D value determination was 55 min, compared to 5 min for the microfluidic-based PC biosensor (Fig. 5). While the microfluidic chip-based assay was run for 5 min, the actual time required for reaction rate constant determination is even less for the initial rate analysis since only a few data points are required after the analyte introduction. Initial rate analysis was used to determine the reaction rate constant because of its simplicity compared to exponentially fitting full association profiles and the need for less data points and thus less data collection time. Analyzing the initial portion of the association/dissociation profiles corresponds to binding of only a small fraction of analytes and therefore allows analysis before steric crowding, analyte depletion or mass transport effects become dominant [26]. Therefore, complications arising from non-ideal behavior associated with binding of biomolecules are reduced.

VI. CONCLUSION

In this work, we have developed a PC biosensor integrated microfluidic chip for measuring biomolecular interaction information. The device's capability to determine kinetic binding information was verified through a heparin-lactoferrin concentration series assay using a detection instrument capable of measuring sensor response at high spatial resolution. The microfluidic device reported in this work incorporates the traditional advantages of flow-channel-based biosensor assays, such as low reagent consumption and rapid response time. The plastic-based replica molding fabrication approach would enable the sensor structure to be inexpensively manufactured and features an external fluid interface that matches a 384-well microplate footprint, and is thus readily compatible with liquid handling infrastructure that is most commonly available within life science laboratories.

ACKNOWLEDGMENT

The authors are grateful to D. Puff at SRU Biosystems for writing the software that enables the kinetic measurements to be performed on the detection instrument. They also gratefully acknowledge SRU Biosystems, the staff of the Micro and Nanotechnology Laboratory, and the Center for Nanoscale Chemical-Electrical—Mechanical Manufacturing Systems (Nano-CEMMS) at the University of Illinois at Urbana–Champaign.

REFERENCES

[1] D. Janasek, J. Franzke, and A. Manz, "Scaling and the design of miniaturized chemical-analysis systems," *Nature*, vol. 442, pp. 374–380, 2006.
[2] N.-T Nguyen and S. T. Wereley, *Fundamentals and Applications of Microfluidics*. Norwood, MA: Artech House, 2002.
[3] P. Yager, T. Edwards, E. Fu, K. Helton, K. Nelson, M. R. Tam, and B. H. Weigl, "Microfluidic diagnostic technologies for global public health," *Nature*, vol. 442, pp. 412–418, 2006.
[4] B. Cunningham, P. Li, B. Lin, and J. Pepper, "Colorimetric resonant reflection as a direct biochemical assay technique," *Sens. Actuators B-Chem.*, vol. 81, pp. 316–328, 2002.
[5] B. Cunningham, B. Lin, J. Qiu, P. Li, J. Pepper, and B. Hugh, "A plastic colorimetric resonant optical biosensor for multiparallel detection of label-free biochemical interactions," *Sens. Actuators B-Chem.*, vol. 85, pp. 219–226, 2002.
[6] B. T. Cunningham and L. Laing, "Microplate-based, label-free detection of biomolecular interactions: Applications in proteomics," *Expert Review of Proteomics*, vol. 3, pp. 271–281, 2006.
[7] B. T. Cunningham, P. Li, S. Schulz, B. Lin, C. Baird, J. Gerstenmaier, C. Genick, F. Wang, E. Fine, and L. Laing, "Label-free assays on the BIND system," *J. Biomolecular Screening*, vol. 9, pp. 481–490, 2004.
[8] L. L. Chan, M. Pineda, J. T. Heeres, P. J. Hergenrother, and B. T. Cunningham, "A general method for discovering inhibitors of protein-DNA interactions using photonic crystal biosensors," *ACS Chem. Biol.*, vol. 3, pp. 437–448, 2008.
[9] B. Lin, P. Li, and B. T. Cunningham, "A label-free biosensor-based cell attachment assay for characterization of cell surface molecules," *Sens. Actuators B-Chem.*, vol. 114, pp. 559–564, 2006.
[10] B. Lin, J. Qiu, J. Gerstenmeier, P. Li, H. M. Pien, J. Pepper, and B. Cunningham, "A label-free optical technique for detecting small molecule interactions," *Biosens. Bioelectron.*, vol. 17, pp. 827–834, 2002.
[11] L. L. Chan, S. L. Gosangari, K. L. Watkin, and B. T. Cunningham, "A label-free photonic crystal biosensor imaging method for detection of cancer cell cytotoxicity and proliferation," *Apoptosis*, vol. 12, pp. 1061–1068, 2007.
[12] U. Jonsson, L. Fagerstam, B. Ivarsson, B. Johnsson, R. Karlsson, K. Lundh, S. Lofas, B. Persson, H. Roos, I. Ronnberg, S. Sjolander, E. Stenberg, R. Stahlberg, C. Urbaniczky, H. Ostlin, and M. Malmqvist, "Real-time biospecific interaction analysis using surface-plasmon resonance and a sensor chip technology," *Biotechniques*, vol. 11, p. 620, 1991.
[13] S. Lofas, M. Malmqvist, I. Ronnberg, E. Stenberg, B. Liedberg, and I. Lundstrom, "Bioanalysis with surface-plasmon resonance," *Sens. Actuators B-Chem.*, vol. 5, pp. 79–84, 1991.

[14] M. A. Cooper, "Label-free screening of bio-molecular interactions," *Anal. Bioanal. Chem.*, vol. 377, pp. 834–842, 2003.
[15] S. K. Lee, S. G. Park, J. H. Moon, and S. M. Yang, "Holographic fabrication of photonic nanostructures for optofluidic integration," *Lab on a Chip*, vol. 8, pp. 388–391, 2008.
[16] H. Y. Zhu, I. M. White, J. D. Suter, and X. D. Fan, "Phage-based label-free biomolecule detection in an opto-fluidic ring resonator," *Biosens. Bioelectron.*, vol. 24, pp. 461–466, 2008.
[17] C. J. Choi and B. T. Cunningham, "A 96-well microplate incorporating a replica molded microfluidic network integrated with photonic crystal biosensors for high throughput kinetic biomolecular interaction analysis," *Lab on a Chip*, vol. 7, pp. 550–556, 2007.
[18] R. Magnusson and S. S. Wang, "New principle for optical filters," *Applied Phys. Lett.*, vol. 61, pp. 1022–1024, 1992.
[19] D. Rosenblatt, A. Sharon, and A. A. Friesem, "Resonant grating waveguide structures," *IEEE J. Quantum Electron.*, vol. 33, pp. 2038–2059, 1997.
[20] C. J. Choi and B. T. Cunningham, "Single-step fabrication and characterization of photonic crystal biosensors with polymer microfluidic channels," *Lab on a Chip*, vol. 6, pp. 1373–1380, 2006.
[21] P. Y. Li, L. Bo, J. Gerstenmaier, and B. T. Cunningham, "A new method for label-free imaging of biomolecular interactions," *Sens. Actuators B-Chem.*, vol. 99, pp. 6–13, 2004.
[22] E. H. Conrad*, Heparin-Binding Proteins*. San Diego, CA: Academic, 1998.
[23] R. I. W. Osmond, W. C. Kett, S. E. Skett, and D. R. Coombe, "Protein-heparin interactions measured by biacore 2000 are affected by the method of heparin immobilization," *Anal. Biochem.*, vol. 310, pp. 199–207, 2002.
[24] S. Zou, C. E. Magura, and W. L. Hurley, "Heparin-binding properties of lactoferrin and lysozyme," *Comparative Biochem. Phys. B-Biochem. Molecular Biol.*, vol. 103, pp. 889–895, 1992.
[25] W. Zhang, N. Ganesh, I. D. Block, and B. T. Cunningham, "High sensitivity photonic crystal biosensor incorporating nanorod structures for enhanced surface area," *Sens. Actuators B-Chem.*, vol. 131, pp. 279–284, 2008.
[26] P. R. Edwards and R. J. Leatherbarrow, "Determination of association rate constants by an optical biosensor using initial rate analysis," *Anal. Biochem.*, vol. 246, pp. 1–6, 1997.

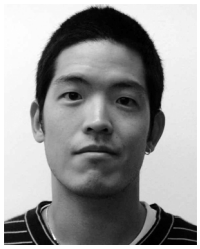

Charles J. Choi received the B.S. degree and the M.S. degree in electrical and computer engineering from the University of Illinois at Urbana–Champaign, Urbana, in 2005 and 2007, respectively. He is currently working towards the Ph.D. degree as a Graduate Research Assistant under the direction of Prof. Brian T. Cunningham at the University of Illinois at Urbana-Champaign.

His research focuses on the design and characterization of optical biosensors and the optimization of detection sensitivity through integration with microfluidics.

Ian D. Block received the B.S. degree in electrical and computer engineering from Cornell University, Ithaca, NY, in 2004, and the M.S. and Ph.D. degrees in electrical and computer engineering from the University of Illinois at Urbana-Champaign. Urbana, in 2005 and 2009, respectively.

His research at the University of Illinois at Urbana-Champaign under the direction of Dr. B. Cunningham focused on the design and characterization of photonic crystal biosensors and supporting instrumentation. He is currently with LS Instruments, Fribourg, Switzerland, working on instrumentation for dynamic light scattering.

Brian Bole, photograph and biography not available at the time of publication.

David Dralle, photograph and biography not available at the time of publication.

Brian T. Cunningham (M'02–SM'07) received the B.S., M.S., and Ph.D. degrees in electrical and computer engineering from the University of Illinois at Urbana– Champaign, Urbana. His thesis research was in the field of optoelectronics and compound semiconductor material science, where he contributed to the development of crystal growth techniques that are now widely used for manufacturing solid state lasers, and high-frequency amplifiers for wireless communication.

He is an Associate Professor of Electrical and Computer Engineering at the University of Illinois at Urbana–Champaign, where he is the Director of the Nano Sensors Group. His group focuses on the development of photonic crystal-based transducers, plastic-based fabrication methods, and novel instrumentation approaches for label-free biodetection. He is a founder and the Chief Technical Officer of SRU Biosystems, Woburn, MA, a life science tools company that provides high sensitivity plastic-based optical biosensors, instrumentation, and software to the pharmaceutical, academic research, genomics, and proteomics communities. Prior to founding SRU Biosystems in June, 2000, he was the Manager of Biomedical Technology at Draper Laboratory, Cambridge, MA, where he directed R&D projects aimed at utilizing defense-related technical capabilities for medical applications. In addition, he served as Group Leader for MEMS Sensors at Draper Laboratory, where he directed a group performing applied research on microfabricated inertial sensors, acoustic sensors, optical switches, microfluidics, tissue engineering, and biosensors. Concurrently, he was an Associate Director of the Center for Innovative Minimally Invasive Therapy (CIMIT), a Boston-area medical technology consortium, where he led the Advanced Technology Team on Microsensors. Before working at Draper Laboratory, he spent five years at the Raytheon Electronic Systems Division developing advanced infrared imaging array technology for defense and commercial applications.